Delineating Local Electromigration for Nanoscale Probing of Lithium Ion Intercalation and Extraction by Electrochemical Strain Microscopy

Qian Nataly Chen [1], Yanyi Liu [2], Yuanming Liu [1], Shuhong Xie [1,3], Guozhong Cao [2], and Jiangyu Li [1,*]

[1] Department of Mechanical Engineering, University of Washington, Seattle, WA 98195, USA

[2] Department of Materials Science and Engineering, University of Washington, Seattle, WA 98195, USA

[3] Key Laboratory of Low Dimensional Materials and Application Technology of Ministry of Education, and Faculty of Materials, Optoelectronics and Physics, Xiangtan University, Xiangtan, Hunan 411105, China

Abstract

Lithium (Li) ion intercalation and extraction are critically important for high performance Li-ion batteries, and they are highly sensitive to local crystalline morphologies and defects that remains poorly understood. Using electrochemical strain microscopy (ESM) in combination with local transport analysis, we demonstrate that we cannot only probe Li-ion concentration and diffusivity with nanometer resolution, but also map local energy dissipation associated with electromigration of Li-ions. Using these techniques, we uncover drastic difference in ESM response and energy dissipation between micro- and nano-crystalline $LiFePO_4$ under different charging states, which explains superior capacity observed in Li-ion batteries with nanocrystalline $LiFePO_4$ electrode.

[*] Author to whom the correspondence should be addressed to; Email: jjli@uw.edu.

As the world gradually moves away from traditional gasoline-fueled internal combustion engines and towards environmentally friendly electric vehicles, there is tremendous demand for high performance electric energy storage devices [1], and lithium (Li) ion batteries have emerged as one of the most promising competitors for their high energy density and excellent cycling stability [2]. In recent years, there have been numerous studies on nanostructured electrodes that have led to significant improvements in Li-ion battery performances [3-7], yet the mechanisms responsible for such enhancements are not well understood. Such a fundamental understanding requires local probing and analysis of coupled electrochemistry and mechanics [8-10] in Li-ion battery electrodes with nanometer resolution, and there has been, until recently, a lack of such techniques.

Scanning probe microscopy (SPM) based techniques have been applied to probe Li-ion electrodes [11] through mappings of topography [12-14] or electronic states [15-17] at nanoscale, yet only recently have the Li-ion diffusions in electrode materials been directly probed using electrochemical strain microscopy (ESM) [18-19], similar to the well established piezoresponse force microscopy (PFM) [20-21]. While previous studies have demonstrated the feasibility of ESM in probing electrode materials, including crystalline $LiCoO_2$ [22] and amorphous Si [23], the mechanisms of ESM are not well established, and it is difficult to separate contributions from diffusion and electromigration [23]. The theoretical analyses developed so far have focused primarily on the diffusion process [24], with the Li-ion concentration gradient assumed to be induced by the electrochemical reaction occurring at the interface between SPM tip and electrode sample, and the liquid meniscus formed at the tip-surface junction serving as the Li-ion reservoir. As the process is controlled by electrochemical reaction in addition to diffusion, the data interpretation and its implications for Li-ion battery electrodes are highly nontrivial and not well understood.

To overcome these difficulties, we focus on Li-ion fluctuation dominated by electromigration instead wherein the applied voltage is relative small, and thus the possible electrochemical reactions at the tip-surface junction can be ignored. Under such conditions, the fluctuation of Li-ion concentration is induced solely by the gradient of tip induced electric field, allowing us to probe the local concentration and diffusivity of Li-ions with nanometer resolution, as validated by careful relaxation studies. The technique was then applied to understand Li-ion intercalation in lithium iron phosphate ($LiFePO_4$) with different crystalline morphologies, which has been extensively investigated in recent years for its high capacity, high power density, abundant material sources, low costs, and low toxicity [25-28]. Indeed, much higher ESM responses have been observed in nanocrystalline $LiFePO_4$, which correlates well with

much enhanced macroscopic performance in Li-ion batteries with nanocrystalline $LiFePO_4$ electrode [29]. Further analysis reveals that Li-ion redistribution in nanocrystalline $LiFePO_4$ shows much smaller energy dissipation and thus smaller energy barriers for Li-ion intercalation and extraction, which explains the substantial performance enhancement often observed in nanostructured electrodes.

Lithium iron phosphate ($LiFePO_4$) was prepared following a sol-gel process previously reported [30], as detailed in the Supplementary Information [31], resulting in an inhomogeneous film consisting of both nano- and micro-crystalline areas, as shown in the scanning electron microscopy (SEM) image in Fig. S1(a). Portions of the film are microcrystalline with distinct facet planes (Fig. S1(b)), while other portions of the film are composed of nanocrystalline sizes with no clear facet plane (Fig. S1(c)). The resulting inhomogeneous cathode exhibits a high initial capacity of 160 mAh/g, as shown in Fig. S1(d), and the corresponding atomic force microscopy (AFM) topography mappings of micro- and nano-crystalline areas are shown in Figs. S1(e) and S1(f). This inhomogeneous film thus provides us a single specimen to probe local electrochemical activities of $LiFePO_4$ with different crystalline morphologies under otherwise identical conditions using ESM. To this end, a 3V AC voltage is applied to the sample through a conductive SPM tip that induces local fluctuation in Li-ion concentration, as schematically shown in Fig. 1(a). The concentration fluctuation is translated into surface vibration due to changes in molar volume [32], which is then recorded by photodiode, making it possible to map the local electrochemical strain with nanometer resolution. A representative ESM amplitude mapping on as-processed $LiFePO_4$ is shown in Fig. 1(b), where ESM responses on the order of 100 pm is observed in the microcrystalline area. Since intrinsic ESM responses are usually small, AC voltage is applied near the cantilever-sample resonance to enhance sensitivity, magnifying such response by orders of magnitude, as shown by three representative resonance peaks at three different locations in Fig. 1(c). Since resonant frequency often shifts with respect to location due to its sensitivity to surface morphology and structural heterogeneity, a dual frequency resonance tracking (DFRT) technique [33-35] is adopted to track the resonance as it shifts during scanning. This also makes it possible to simultaneously determine the quality factor Q using the damped harmonic oscillator model [34], and thus determine the intrinsic ESM amplitude mapping by correcting the resonance magnification with quality factor, as shown in Fig. 1(d) overlaid on three-dimensional (3D) topography, where much smaller ESM amplitudes on the order of 1 pm are observed after correction. The corresponding mappings of quality factor and resonance frequency are shown in Figs. 1(e) and 1(f). Finally, we also

note that there is little phase contrast in the mapping, which differs from typical PFM because the opposite polarities that commonly exist in ferroelectrics are not found in Li-ion electrodes.

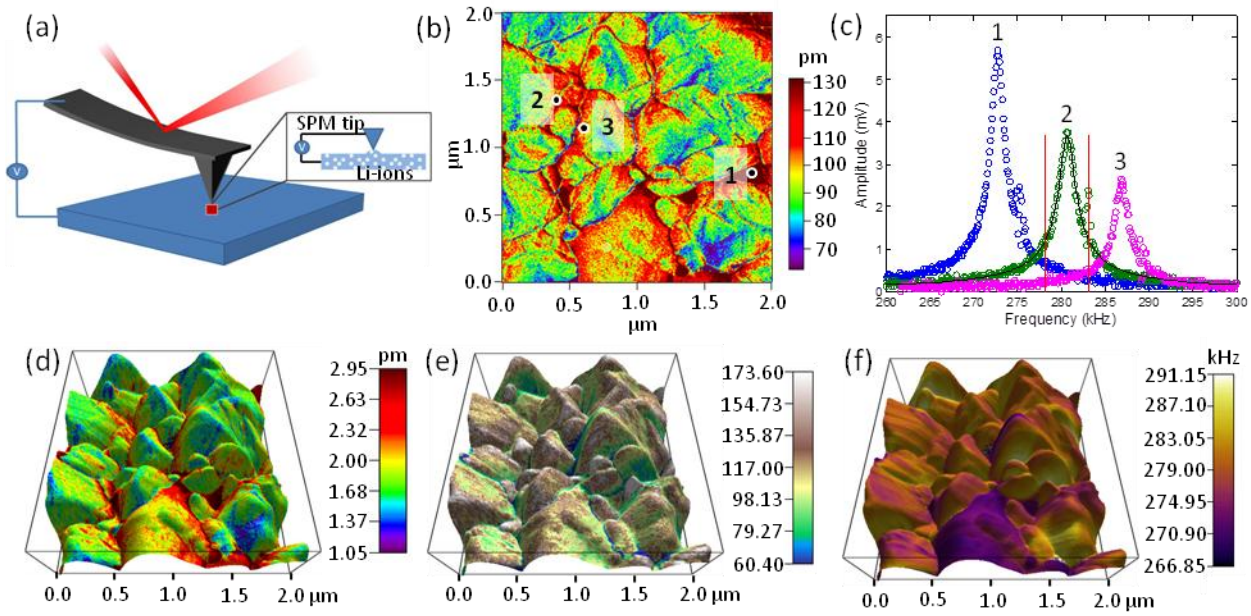

Figure 1: Electrochemical strain microscopy (ESM) of $LiFePO_4$ nanocrystals; (a) the schematic illustration of ESM; (b) ESM amplitude mapping before resonance correction; (c) resonance peaks at three locations, and the schematics of DFRT using actual experimental data; and mappings of (d) corrected ESM amplitude; (e) quality factor; and (f) resonant frequency, all overlaid on 3D topography.

In order to understand the electrochemical implications of ESM response, we examine the transport of Li-ions in electrodes in more detail. For small perturbations under SPM induced electric field, it is assumed that the redistribution of Li-ion concentration *n* is governed by [36],

$$\frac{\partial n}{\partial t} = \nabla \cdot (D \nabla n) + \nabla \cdot \left(\frac{DzFn}{RT} \nabla \varphi \right), \tag{1}$$

where the first term is the diffusion contribution with *D* being the diffusion coefficient, and the second term is the electromigration contribution. Under equilibrium conditions before SPM probing, both contributions are balanced, and there is no evolution of Li-ion concentration. Since the AC voltage is applied with relatively high frequencies in the range of 100 kHz, much shorter than typical diffusion time scales, and large gradient exists in the tip induced electric field, the redistribution of Li-ion concentration underneath the SPM tip is assumed to be solely due to electromigration, and such small perturbations do not change overall concentration distributions of Li-ions. With such approximations, Eq. (1) can be simplified as

$$\frac{\partial n}{\partial t} = n_0 D \frac{zF}{RT} \nabla^2 \varphi, \quad (2)$$

and it is evident that changes in Li-ion concentration induced by SPM tip is proportional to the local equilibrium concentration n_0 as well as the diffusion coefficient D. Since this change is directly proportional to molar volume change and thus the ESM response probed, we conclude that ESM amplitude also correlates with the local concentration as well as the diffusion coefficient of Li-ion. It is worth mentioning that analyzing ESM signal is highly nontrivial, and our current analysis, although providing great insight, is still semi-phenomenological. More detailed numerical simulation of ESM response is currently ongoing.

In order to verify this analysis and interpretation, we apply a sequence of DC step voltages through the SPM tip to the as-processed, charged, and discharged $LiFePO_4$ films and measure the corresponding ESM responses, as shown in Fig. 2. Initially, the ESM amplitude is measured in the absence of applied DC voltage to establish the response at ground state. Since the response is dominated by electrostatic interactions when DC voltage is on, which leads to ultrahigh amplitudes regardless of DC polarity, we only examine the relaxation of ESM response after the DC voltage is reduced to zero, similar to the relaxation studies of induced polar state in relaxor [37], interfacial ionic conduction in glass ceramics [38], organic solar cells [39], and biological ferroelectricity in aortic walls [40] . In the as-processed sample, a large drop in ESM response is observed immediately after the removal of the positive DC voltage, which then gradually increases back to the ground level before the application of the negative DC voltage, as shown in Fig. 2(a). On the other hand, after the removal of a negative DC voltage, a large increase in ESM amplitude is observed, which gradually decreases to the ground state. The different relaxation characteristics under different DC polarities can be clearly understood from our interpretation of ESM responses - a positive DC voltage by SPM tip reduces the Li-ion concentration underneath the SPM tip, resulting in a smaller response than in the ground state, while a negative DC voltage increases the Li-ion concentration underneath the SPM tip, resulting in a larger ESM response. The relaxation of ESM response to ground state after removal of either positive or negative voltage corresponds to the redistribution of Li-ions to the equilibrium concentration at ground state. Such mechanism is further confirmed by relaxation characteristics observed for the charged electrode in Fig. 2(b), where the responses are very close to ground state regardless of DC voltage polarities due to the lack of Li-ions in the charged cathode, and little relaxation is observed after removal of either positive or negative voltages. For the discharged cathode shown in Fig. 2(c), the trend of relaxation is similar to the

as-processed sample, though the variation in ESM magnitude is smaller, which can be understood from well documented capacity loss during the first cycle of charging and discharging [41-42]. While these relaxation studies were conducted on a single point in each sample, the qualitative trend is consistent at different locations. We also point out that according to Eq. (2), the ESM response is linear to the applied AC voltage, which is confirmed by our data shown in Fig. S2, especially under 4 V. Even with continuous application of DC voltage, we did not observe the formation of solid particles that would indicate electrochemical reactions [43].

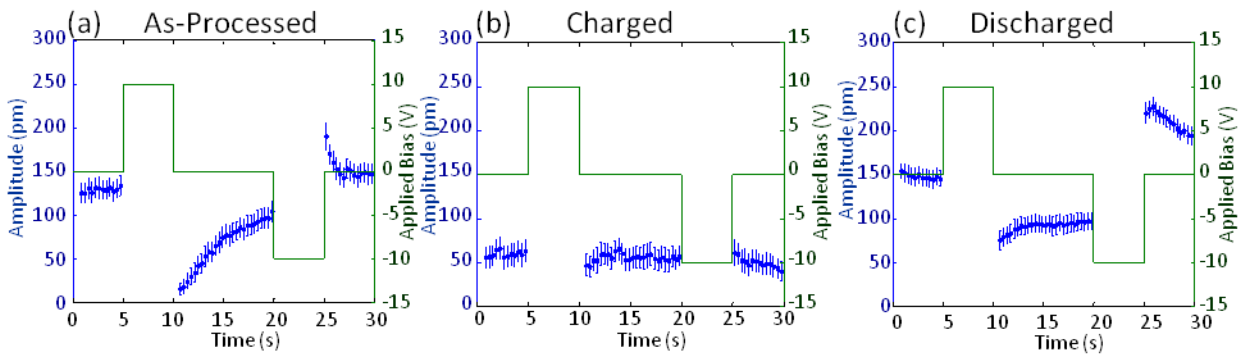

Figure 2: Relaxation characteristics of ESM responses of $LiFePO_4$ electrode at different stages of processing and testing, where the left axis indicates the ESM response and right axis indicates the applied voltage; (a) as processed; (b) charged; and (c) discharged. During the experiment, the amplitude was measured every 0.5 ms, and the data was averaged over every 0.2 s period.

The relaxation characteristics after removal of DC voltages confirm that the ESM response correlates with the local concentration and diffusivity of Li-ions, and this allows us to examine differences in Li-ion intercalation and extraction in $LiFePO_4$ with different crystalline morphologies. The comparison of ESM amplitude mappings for micro- and nano-crystalline $LiFePO_4$ is shown in Fig. 3, obtained using DFRT and corrected by quality factor. The top row maps microcrystalline areas with large crystal sizes in the as-processed, charged, and discharged states, and the bottom row maps the nanocrystalline areas with smaller crystalline sizes correspondingly. Again, the differences among as-processed, charged, and discharged samples are evident, confirming that the responses correlate with Li-ion concentration. Even more importantly, notable ESM contrast between micro- and nano-crystalline areas of large and small crystalline size is observed. In the as-processed sample, the averaged ESM response in the nanocrystalline area is more than twice the response in the microcrystalline area, suggesting that Li-ions in nanocrystalline $LiFePO_4$ have higher diffusivity. After charging, the averaged amplitude drops substantially in both areas due to extraction of Li-ions, though the nanocrystalline area

still shows approximately 20% higher averaged response. In the discharged state, substantially higher ESM response of more than 70% is observed in the nanocrystalline area, which is attributed to both higher Li-ion intercalation and diffusivity. The correlation between nanoscale ESM response and local crystalline morphologies is evident, which may help understand the enhanced performance in Li-ion batteries with nanocrystalline $LiFePO_4$ electrode.

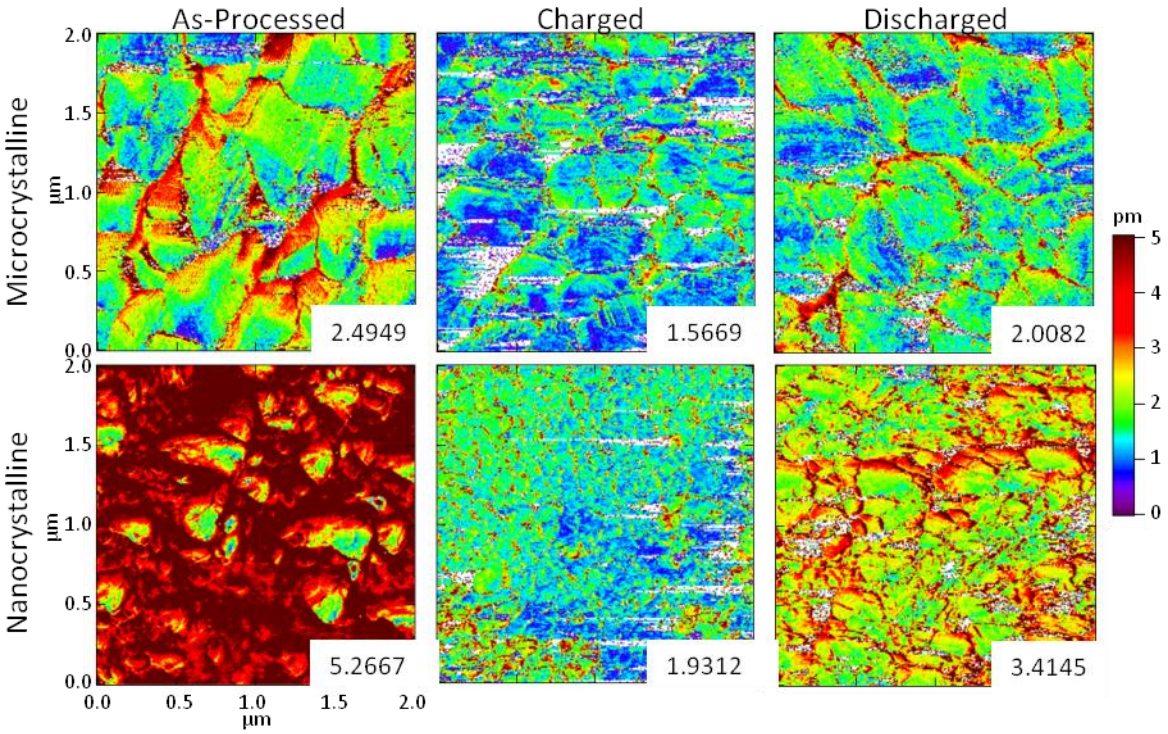

Figure 3: Comparison of corrected ESM amplitude mappings of $LiFePO_4$ electrode in micro- and nano-crystalline areas at different stages of processing and testing, with the averaged amplitude identified in each mapping.

Indeed, it has recently been demonstrated that $LiFePO_4$ film annealed at 600°C on Pt-coated Si shows nanocrystalline morphology similar to Fig. S1(c), and exhibit a superior initial energy capacity of 312 mAh/g, while $LiFePO_4$ film annealed at 800°C shows microcrystalline morphology similar to Fig. S1(b), and possesses a relatively low capacity of 120 mAh/g [30]. Our local ESM studies thus correlates well with such contrast in macroscopic battery performances, and may help understand the mechanisms responsible for performance enhancement in nanocrystalline $LiFePO_4$. To this end, we examine the mappings of quality factor, which is inversely proportional to energy dissipation associated with Li-ion redistribution and thus reflects the energy barrier for Li-ion intercalation and extraction. While the total energy dissipation at each point is directly correlated with the quality factor, the energy dissipation per unit Li-ion redistribution is more significant, and can be analyzed by normalizing the total dissipation

with respect to ESM magnitude, which is directly proportional to redistributed Li-ion concentration. Although we are interested in dissipation originated from ionic motion, it is pointed out that the mechanical dissipation is also included in the data that cannot be separated from ionic effect for the time being. Furthermore, we have ignored the effects of noise background. The mappings of such energy dissipation per unit Li-ion redistribution for micro- and nano-crystalline $LiFePO_4$ under different states are shown in Fig. 4, and the contrast between the micro- and nano-crystalline $LiFePO_4$ is evident. The nanocrystalline region shows substantially smaller energy dissipation compared with the microcrystalline one in as-processed and discharged samples, suggesting much smaller energy barriers for Li-ion intercalation and extraction in nanocrystalline $LiFePO_4$. This difference may be due to the one-dimensional ion transport channel in $LiFePO_4$ [44], for which clear crystalline facets as seen in microcrystalline region might not be desirable when they are misaligned with the transport channel. Indeed, it appears from 3D topography that the dissipation is rather uniform within one facet, yet varying from facet to facet in microcrystalline region in the as-processed state. On the other hand, for nanocrystalline region without clear crystalline facet, the dissipation is rather uniform, especially in the as-processed state.

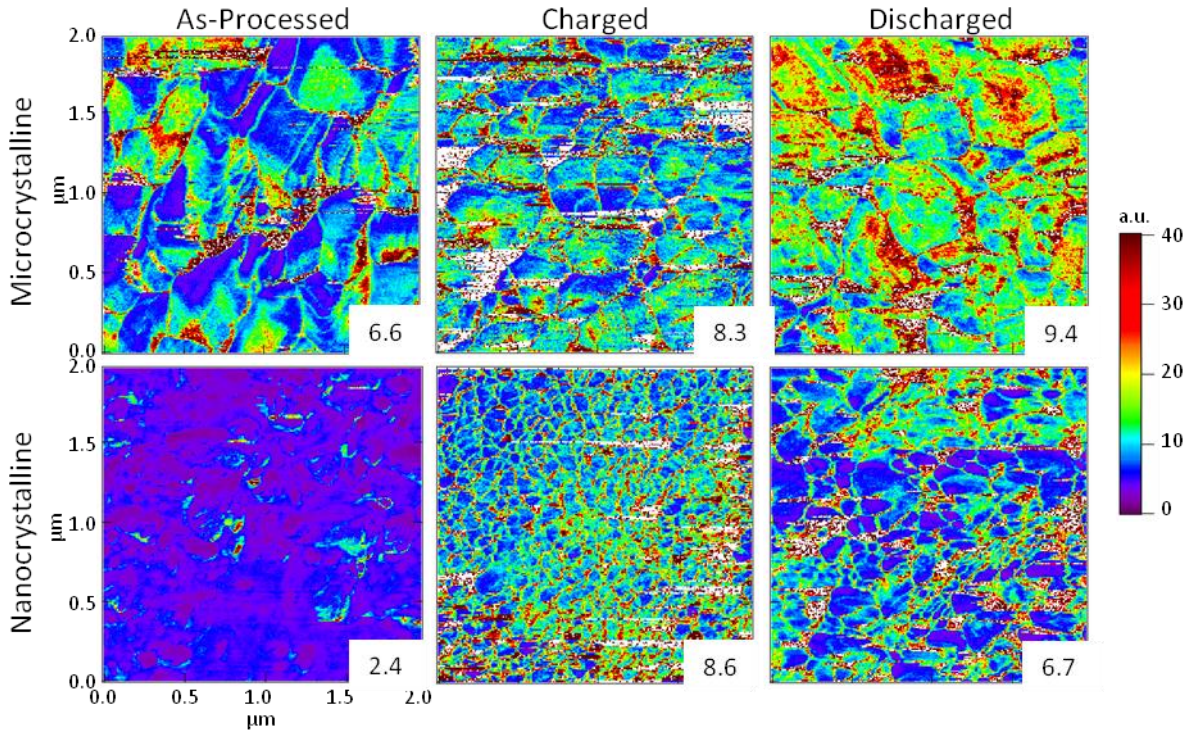

Figure 4: Comparison of ESM dissipation mappings of $LiFePO_4$ electrode in micro- and nano-crystalline areas at different stages of processing and testing, normalized by the respective ESM amplitude, with the averaged dissipation identified in each mapping.

In summary, we have probed local electrochemical strain in inhomogeneous $LiFePO_4$ cathode with nanometer resolution, and established clear correlation between nanoscale Li-ion electrochemical activity and local crystalline morphology on one hand, and macroscopic battery level performance on the other. Not only have the local Li-ion concentration and diffusivity been probed, but also the energy dissipation during Li-ion transport been mapped. It is discovered that nanocrystalline $LiFePO_4$ exhibit higher Li-ion diffusivity and lower energy dissipation than microcrystalline $LiFePO_4$, which explains its higher capacity often observed at macroscopic battery level. This study thus can help understand Li-ion interaction and extraction at nanoscale, particularly their dependence on crystalline morphologies and defects, and can help develop electrode materials for Li-ion batteries with enhanced performance.

Acknowledgement

The authors would like to acknowledge the financial support from National Science Foundation (CMMI 1100339 and DMR 1006194), Natural Science Foundation of China (10972189), and UW TGIF. QNC acknowledges the support of NASA Space Technology Research Fellowship (11-NSTRF11-0323). YML acknowledges partial support of a UIF Fellowship from the Center for Nanotechnology, University of Washington. S.H. Xie acknowledges the support of China Scholarship Council.

References

[1] B. Dunn, H. Kamath, and J. M. Tarascon, Science **334**, 928 (2011).

[2] G. A. Nazri, and G. Pistoia, *Lithium Batteries Science and Technology* (Kluwer Academic Publishers, Dordrecht, Netherlands, 2004).

[3] P. G. Bruce, B. Scrosati, and J. M. Tarascon, Angew. Chem., Int. Ed. **47**, 2930 (2008).

[4] M. G. Kim, and J. Cho, Adv. Funct. Mater. **19**, 1497 (2009).

[5] Y. Wang, and G. Z. Cao, Adv. Mater. **20**, 2251 (2008).

[6] Y. Liu, D. Liu, Q. Zhang, and G. Cao, J. Mater. Chem. **21**, 9969 (2011).

[7] W. Wang, and P. N. Kumta, ACS Nano **4**, 2233 (2010).

[8] S. K. Soni, B. W. Sheldon, X. Xiao, M. W. Verbrugge, D. Ahn, H. Haftbaradaran, and H. Gao, J. Electrochem. Soc. **159**, A38 (2012).

[9] K. J. Zhao, M. Pharr, Q. Wan, W. L. Wang, E. Kaxiras, J. J. Vlassak, and Z. G. Suo, J. Electrochem. Soc. **159**, A238 (2012).

[10] S. Golmon, K. Maute, and M. L. Dunn, Comput. Struct. **87**, 1567 (2009).

[11] S. V. Kalinin, and N. Balke, Adv. Mater. **22**, E193 (2010).

[12] M. Koltypin, Y. S. Cohen, B. Markovsky, Y. Cohen, and D. Aurbach, Electrochem. Commun. **4**, 17 (2002).

[13] L. Y. Beaulieu, V. K. Cumyn, K. W. Eberman, L. J. Krause, and J. R. Dahn, Rev. Sci. Instrum. **72**, 3313 (2001).

[14] L. Y. Beaulieu, T. D. Hatchard, A. Bonakdarpour, M. D. Fleischauer, and J. R. Dahn, J. Electrochem. Soc. **150**, A1457 (2003).

[15] R. O'Hayre, M. Lee, and F. B. Prinz, J. Appl. Phys. **95**, 8382 (2004).

[16] S. Pejovnik, R. Dominko, M. Bele, M. Gaberscek, and J. Jamnik, J. Power Sources **184**, 593 (2008).

[17] R. Shao, S. V. Kalinin, and D. A. Bonnell, Appl. Phys. Lett. **82**, 1869 (2003).

[18] N. Balke, S. Jesse, A. N. Morozovska, E. Eliseev, D. W. Chung, Y. Kim, L. Adamczyk, R. E. Garcia, N. Dudney, and S. V. Kalinin, Nat. Nanotechnol. **5**, 749 (2010).

[19] N. Balke, S. Jesse, Y. Kim, L. Adamczyk, I. N. Ivanov, N. J. Dudney, and S. V. Kalinin, ACS Nano **4**, 7349 (2010).

[20] A. Gruverman, and S. V. Kalinin, J. Mater. Sci. **41**, 107 (2006).

[21] D. A. Bonnell, S. V. Kalinin, A. L. Kholkin, and A. Gruverman, MRS Bull. **34**, 648 (2009).

[22] S. Guo, S. Jesse, S. Kalnaus, N. Balke, C. Daniel, and S. V. Kalinin, J. Electrochem. Soc. **158**, A982 (2011).

[23] N. Balke, S. Jesse, Y. Kim, L. Adamczyk, A. Tselev, I. N. Ivanov, N. J. Dudney, and S. V. Kalinin, Nano Lett. **10**, 3420 (2010).

[24] A. N. Morozovska, E. A. Eliseev, N. Balke, and S. V. Kalinin, J. Appl. Phys. **108**, 053712 (2010).

[25] L. X. Yuan, Z. H. Wang, W. X. Zhang, X. L. Hu, J. T. Chen, Y. H. Huang, and J. B. Goodenough, Energy Environ. Sci. **4**, 269 (2011).

[26] W. J. Zhang, J. Power Sources **196**, 2962 (2011).

[27] A. K. Padhi, K. S. Nanjundaswamy, and J. B. Goodenough, J. Electrochem. Soc. **144**, 1188 (1997).

[28] S. Y. Chung, J. T. Bloking, and Y. M. Chiang, Nat. Mater. **1**, 123 (2002).

[29] C. Delacourt, P. Poizot, S. Levasseur, and C. Masquelier, Electrochem. Solid-State Lett. **9**, A352 (2006).

[30] Y. Liu, D. Liu, Q. Zhang, D. Yu, J. Liu, and G. Cao, Electrochim. Acta **56**, 2559 (2011).

[31] See Supplementary Materials at [ ] for three additional figures and experimental details.

[32] L. Y. Beaulieu, K. W. Eberman, R. L. Turner, L. J. Krause, and J. R. Dahn, Electrochem. Solid-State Lett. **4**, A137 (2001).

[33] B. J. Rodriguez, C. Callahan, S. V. Kalinin, and R. Proksch, Nanotechnology **18**, 475504 (2007).

[34] S. Jesse, B. Mirman, and S. V. Kalinin, Appl. Phys. Lett. **89**, 022906 (2006).

[35] S. H. Xie, A. Gannepalli, Q. N. Chen, Y. M. Liu, Y. C. Zhou, R. Proksch, and J. Y. Li, Nanoscale **4**, 408 (2012).

[36] R. E. Garcia, Y. M. Chiang, W. C. Carter, P. Limthongkul, and C. M. Bishop, J. Electrochem. Soc. **152**, A255 (2005).

[37] V. V. Shvartsman, A. L. Kholkin, M. Tyunina, and J. Levoska, Appl. Phys. Lett. **86**, 222907 (2005).

[38] A. Schirmeisen, A. Taskiran, H. Fuchs, H. Bracht, S. Murugavel, and B. Roling, Phys. Rev. Lett. **98**, 225901 (2007).

[39] D. C. Coffey, and D. S. Ginger, Nat. Mater. **5**, 735 (2006).

[40] Y. Liu, Y. Zhang, M.-J. Chow, Q. N. Chen, and J. Li, Phys. Rev. Lett. **108**, 078103 (2012).

[41] A. S. Andersson, and J. O. Thomas, J. Power Sources **97-8**, 498 (2001).

[42] Y. Matsumura, S. Wang, and J. Mondori, J. Electrochem. Soc. **142**, 2914 (1995).

[43] T. M. Arruda, A. Kumar, S. V. Kalinin, and S. Jesse, Nano Lett. **11**, 4161 (2011).

[44] D. Morgan, A. Van der Ven, and G. Ceder, Electrochem. Solid-State Lett. **7**, A30 (2004).